INTERNATIONAL JOURNAL FOR NUMERICAL METHODS IN FLUIDS
Int. J. Numer. Meth. Fluids 2006; **52**:679–705
Published online 13 March 2006 in Wiley InterScience (www.interscience.wiley.com). DOI: 10.1002/fld.1200

The multi-stage centred-scheme approach applied to a drift-flux two-phase flow model

Svend Tollak Munkejord[1,*,†], Steinar Evje[2,‡] and Tore Flåtten[2,§,¶]

[1]*Norwegian University of Science and Technology* (*NTNU*), *Department of Energy and Process Engineering*, *Kolbjørn Hejes veg 1A*, *NO-7491 Trondheim*, *Norway*
[2]*International Research Institute of Stavanger* (*IRIS*), *Prof. Hanssensvei 15*, *Stavanger*, *Norway*

SUMMARY

For two-phase flow models, upwind schemes are most often difficult do derive, and expensive to use. Centred schemes, on the other hand, are simple, but more dissipative. The recently proposed multi-stage (MUSTA) method is aimed at coming close to the accuracy of upwind schemes while retaining the simplicity of centred schemes. So far, the MUSTA approach has been shown to work well for the Euler equations of inviscid, compressible single-phase flow. In this work, we explore the MUSTA scheme for a more complex system of equations: the drift-flux model, which describes one-dimensional two-phase flow where the motions of the phases are strongly coupled. As the number of stages is increased, the results of the MUSTA scheme approach those of the Roe method. The good results of the MUSTA scheme are dependent on the use of a large-enough local grid. Hence, the main benefit of the MUSTA scheme is its simplicity, rather than CPU-time savings. Copyright © 2006 John Wiley & Sons, Ltd.

KEY WORDS: two-phase flow; drift-flux model; MUSTA scheme; centred scheme

1. INTRODUCTION

Multiphase flows are important in a large range of industrial applications, such as in the oil and gas industry, in the chemical and process industry, including in heat-pumping systems, as well as in the safety analysis of nuclear power plants.

Depending on the problem at hand, the desired level of detail, and the computational resources available, a range of techniques are employed for the numerical simulation of these

*Correspondence to: S. T. Munkejord, NTNU, Department of Energy and Process Engineering, Kolbjørn Hejes veg 1A, NO-7491 Trondheim, Norway.
†E-mail: stm@pvv.ntnu.no
‡E-mail: Steinar.Evje@irisresearch.no
§E-mail: Tore.Flaatten@irisresearch.no
¶Current address: Centre of Mathematics for Applications, 1053 Blindern, NO-0316 Oslo, Norway.

Contract/grant sponsor: Research Council of Norway

Received 24 October 2005
Revised 19 January 2006
Accepted 22 January 2006

flows. Here we consider a *drift-flux* model, which is a two-phase model arising from averaging the equations for single-phase flow (see Reference [1]). It consists of a continuity equation for each phase, and a momentum equation for the mixture, and it is employed to describe bubbly flows and other two-phase flows where the motions of the phases are strongly coupled.

For such *mixed* flow regimes, the drift-flux model presents several advantages. In addition to providing a physically realistic description of various two-phase propagation phenomena [2–4], it represents a mathematical simplification compared to more general two-fluid models [5]. For these reasons, the model has been used in several industrial computer codes, such as the TACITE code [6] developed for the petroleum industry.

Since the momentum equation is for the two-phase mixture, a supplementary *hydrodynamic closure law*, commonly denoted as the *slip relation*, is required to determine the velocity of each phase. In addition, *thermodynamic closure laws* are needed for each phase to relate the phasic density to the mixture pressure. The drift-flux model can be written on conservation form, and it has shown to be hyperbolic for a reasonable range of input parameters [7]. However, even for simple closure relations, the Jacobian of the model becomes rather complicated.

1.1. Riemann solvers

A popular class of methods for solving systems of hyperbolic equations for flow problems are the Godunov-type methods (see, e.g. References [8, 9] for a review). The basic scheme involves the solution of the Riemann problem at each cell interface. This solution is used to compute the intercell flux. Since they employ wave-propagation information in the construction of the numerical flux, these schemes are often called *upwind* or *upstream* schemes. The Riemann problem can be exactly solved for models such as the Euler equations of inviscid, compressible single-phase flow. However, an exact Riemann solution for the drift-flux model may be derived only for some special cases, since the model is sensitive to the formulation of the closure laws.

It is often adequate to employ an approximate Riemann solver. An attractive candidate is that of Roe [10], in which the original model is linearized at each cell interface, and a representation of all the wave phenomena in the model is provided. To that end, the Jacobian of the model is diagonalized.

As has been pointed out by several researchers [7, 11–15], the complexity resulting from the closure laws employed in the drift-flux model severely restricts the possibilities for constructing a Roe solver by purely algebraic manipulations. Nevertheless, Roe-type schemes have been proposed for this model. Romate [7] presented a method for constructing a Roe matrix using a fully numerical approach, whereas Flåtten and Munkejord [16] derived an analytical Roe matrix for fairly general closure laws. Still, their approach relied on a numerical diagonalization of the Roe matrix, and on the closure laws not including differential terms. Such terms were discussed, e.g. by Bouré [3].

1.2. Centred schemes

A simpler method for calculating the intercell flux is to employ *centred* stencils, which do not explicitly make use of wave-propagation information in the construction of the numerical flux. However, the centred schemes are generally more dissipative than the upwind ones (see, e.g. Reference [9]).

The FORCE flux has been proposed by Toro as an interesting basic centred flux, and it is known that the FORCE scheme possesses various good properties [9, 17, 18]. It has been shown to be monotone, to possess the optimal stability condition, and to have the smallest numerical viscosity among centred schemes when it is considered for a scalar, linear conservation law. Moreover, entropy consistence has also been shown for a general non-linear system of conservation laws, and convergence results have been obtained for special systems like the isentropic Euler equations and the shallow-water equations [17].

However, a main drawback of FORCE is clearly observed when considering its truncation error for a linear advection equation with constant speed a; $\partial u/\partial t + a\,\partial u/\partial x = 0$. In this case, the truncation error is inversely proportional to the Courant–Friedrichs–Lewy (CFL) number $C = a\Delta t/\Delta x$ [19]. In particular, the FORCE scheme cannot resolve a stationary discontinuity exactly.

1.3. The multi-stage approach

The multi-stage (MUSTA) method proposed by Titarev and Toro [19], Toro [20] is aimed at coming close to the accuracy of upwind schemes while retaining the simplicity of centred schemes. In this approach, the solution of the Riemann problem at the cell interface is approximated numerically by employing a first-order centred scheme on a local grid. More precisely, by using $2N$ spatial grid cells, M local time steps, and a local CFL number, $C_{\mathrm{loc}} = a\Delta t_{\mathrm{loc}}/\Delta x$, Titarev and Toro [19] showed that the truncation error for the linear advection equation with constant wave speed could be strongly reduced. In particular, this MUSTA scheme was demonstrated to behave similarly to the upwind Godunov scheme for the linear advection equation. Motivated by this, the authors applied their scheme to the Euler equations and observed that the new MUSTA scheme could effectively match the accuracy of the Godunov method with state-of-the-art Riemann solvers.

An important motivation for the development of the MUSTA scheme was the possibility to use it for more complex systems, such as those occurring in multiphase fluid dynamics. The main purpose of this work is to take one step in this direction.

The analysis behind the construction of the MUSTA scheme proposed by Titarev and Toro [19] is based on the linear advection equation and monotonicity considerations related to this simple equation. Therefore, it may not be obvious that the good properties of the MUSTA scheme for the scalar case in fact carry over to the case of more complicated systems of conservation laws. Titarev and Toro demonstrated that the MUSTA scheme works well for the Euler equations. However, in order to resolve the local Riemann problem, appropriate choices are needed for the parameters M and N for the local grid. These depend on the specific model under consideration. Consequently, there is a need for exploring the MUSTA approach also for other models than the Euler equations. The aim of this work is thus to explore the MUSTA approach for a two-phase model, the drift-flux model, and reveal more insight into the potential of this approach when it is applied to a relatively complicated system.

1.4. The drift-flux model

A main feature of the drift-flux model is that it possesses two fast waves (sound waves) and one slowly moving wave (mass wave). In particular, if we have a transition from two-phase to pure liquid flow, the speed of sound can change from the order of 10 m/s to the order of 1000 m/s. Consequently, for such flow scenarios (which are highly relevant for

the petroleum industry), one is forced to take very small time steps according to the CFL condition. A main purpose of this work is to demonstrate to what extent the improved MUSTA scheme of Titarev and Toro [19] is able to give an accurate resolution of the important slowly moving mass waves. Due to the possible large gap between the smallest and largest eigenvalues, the drift-flux model may represent a harder test for the MUSTA scheme than the Euler equations. Specifically, we also want to explore in what way the resolution properties of the MUSTA scheme depend on choices related to the local grid represented by the parameters M and N.

The rest of this paper is organized as follows. In Section 2, the drift-flux model is described. The numerical algorithm, including a second-order extension, is detailed in Section 3. Section 4 presents numerical simulations aimed at demonstrating the accuracy and robustness properties of the MUSTA scheme, as well as to highlight the importance of the involved parameters. Further, the section shows the differences between the MUSTA scheme and the Roe scheme. The main results are summarized in Section 5, and conclusions drawn in Section 6.

2. THE DRIFT-FLUX MODEL

This section describes the employed drift-flux model along with its closure laws, as well as wave-speed estimates.

2.1. Model formulation

The model under consideration may be written in the following vector form:

$$\frac{\partial \mathbf{q}}{\partial t} + \frac{\partial \mathbf{f}(\mathbf{q})}{\partial x} = \mathbf{s}(\mathbf{q}) \tag{1}$$

where $\mathbf{q}$ is the vector of conserved variables, $\mathbf{f}$ is the vector of fluxes, and $\mathbf{s}(\mathbf{q})$ is the vector of sources. They are given by

$$\mathbf{q} = \begin{bmatrix} \rho_g \alpha_g \\ \rho_\ell \alpha_\ell \\ \rho_g \alpha_g u_g + \rho_\ell \alpha_\ell u_\ell \end{bmatrix} \tag{2}$$

$$\mathbf{f}(\mathbf{q}) = \begin{bmatrix} \rho_g \alpha_g u_g \\ \rho_\ell \alpha_\ell u_\ell \\ \rho_g \alpha_g u_g^2 + \rho_\ell \alpha_\ell u_\ell^2 + p \end{bmatrix} \tag{3}$$

and

$$\mathbf{s}(\mathbf{q}) = \begin{bmatrix} 0 \\ 0 \\ -F_w \end{bmatrix} \tag{4}$$

2.1.1. Nomenclature. In the following, we use the index $k \in \{\mathrm{g}, \ell\}$ to denote either the gas (g) or liquid (ℓ) phase. For each phase, the variables are defined as follows: α_k is the density; u_k is the velocity; α_k is the volume fraction; p is the pressure common to both phases and F_{w} is the wall-friction momentum source.

The volume fractions satisfy

$$\alpha_{\mathrm{g}} + \alpha_{\ell} = 1 \tag{5}$$

Mass transfer between the phases is not considered. Further, dynamic energy transfers are neglected; we consider isentropic or isothermal flows. In particular, this means that the pressure may be obtained as

$$p = p(\rho_{\mathrm{g}}) = p(\rho_{\ell}) \tag{6}$$

2.1.2. Thermodynamic submodels. For the numerical simulations presented in this work, we assume that both the gas and liquid phases are compressible, described by the simplified thermodynamic relations

$$\rho_{\ell} = \rho_{\ell,0} + \frac{p - p_{\ell,0}}{c_{\ell}^2} \tag{7}$$

and

$$\rho_{\mathrm{g}} = \rho_{\mathrm{g},0} + \frac{p - p_{\mathrm{g},0}}{c_{\mathrm{g}}^2} \tag{8}$$

where

$$p_{k,0} = p(\rho_{k,0})$$

and the reference density $\rho_{k,0}$ and speed of sound c_k are constants for each phase k.

2.1.3. Hydrodynamic submodels. By far, the most important aspect of the model is the *hydrodynamic closure law*, which is commonly expressed in the following general form:

$$u_{\mathrm{g}} - u_{\ell} = \Phi(\alpha_{\mathrm{g}}, p, u_{\mathrm{g}}) \tag{9}$$

A special case of interest is the Zuber and Findlay [21] relation

$$u_{\mathrm{g}} = K(\alpha_{\mathrm{g}} u_{\mathrm{g}} + \alpha_{\ell} u_{\ell}) + S \tag{10}$$

where K and S are flow-dependent parameters. The validity of (10) has been experimentally established for a broad range of parameters for both bubbly and slug flows [2, 4, 22].

In the following calculations, the wall-friction term, F_{w}, is set equal to 0 unless otherwise stated.

2.1.4. Wave-speed estimates. To obtain the local and global time-step lengths, it is necessary to employ the CFL criterion. The CFL number is

$$C = \frac{\|\lambda\|_{\infty} \Delta t}{\Delta x} \tag{11}$$

where $\|\lambda\|_\infty$ is the maximum eigenvalue of the Jacobian matrix of the model (1) in the computational domain. This shows that even though no information of the eigenstructure of the model is directly used in the calculation of the MUSTA flux, an estimate of the maximum eigenvalue is still needed. The approximate eigenvalues used here are given in Appendix A. It should be noted that the computed results are not very sensitive to the eigenvalue estimate. For instance, we have carried out some experiments using the simple estimate by Evje and Fjelde [14] based on a no-slip assumption, and only minor differences were observed in the numerical results.

3. NUMERICAL ALGORITHM

The drift-flux model written in the form (1) can be integrated over a control volume to yield the semi-discrete formulation

$$\frac{\mathrm{d}}{\mathrm{d}t}\mathbf{Q}_i(t) = -\frac{1}{\Delta x}(\mathbf{F}_{i+1/2} - \mathbf{F}_{i-1/2}) + \mathbf{S}_i \tag{12}$$

A simple way of integrating (12) in time is to use the forward Euler method:

$$\mathbf{Q}_i^{j+1} - \mathbf{Q}_i^j = -\frac{\Delta t}{\Delta x}(\mathbf{F}_{i+1/2} - \mathbf{F}_{i-1/2}) + \Delta t\mathbf{S}_i \tag{13}$$

Herein, $\mathbf{Q}_i^j$ denotes the numerical approximation to the cell average of the vector of unknowns, $\mathbf{q}(x(i), t_j)$, that is, in control volume i at time step j. Quantities without a time index are evaluated at time step j.

A method for specifying the cell fluxes $\mathbf{F}_{i-1/2}$ is needed. In the Godunov method, the solution of the local Riemann problem at the cell interfaces is employed. For two-phase flow models, an exact solution to the Riemann problem is not easy to find. Even the derivation of approximate Riemann solvers, such as those of the type of Roe [10], involves a good deal of work.

3.1. *FORCE flux*

A simple method for calculating the numerical flux $\mathbf{F}_{i-1/2}$ is to use the first-order centred (FORCE) scheme of Toro [9, Section 14.5.1]. We restate it here for completeness. The FORCE flux is given by

$$\mathbf{F}_{i-1/2} = \tfrac{1}{2}(\mathbf{F}^{\mathrm{LF}}_{i-1/2} + \mathbf{F}^{\mathrm{Ri}}_{i-1/2}) \tag{14}$$

where $\mathbf{F}^{\mathrm{LF}}_{i-1/2}$ is the Lax–Friedrichs flux

$$\mathbf{F}^{\mathrm{LF}}_{i-1/2} = \tfrac{1}{2}(\mathbf{f}(\mathbf{Q}_{i-1}) + \mathbf{f}(\mathbf{Q}_i)) - \frac{1}{2}\frac{\Delta x}{\Delta t}(\mathbf{Q}_i - \mathbf{Q}_{i-1}) \tag{15}$$

and $\mathbf{F}^{\mathrm{Ri}}_{i-1/2}$ is the Richtmyer flux. It is computed by first defining an intermediate state

$$\mathbf{Q}^{\mathrm{Ri}}_{i-1/2} = \tfrac{1}{2}(\mathbf{Q}_{i-1} + \mathbf{Q}_i) - \frac{1}{2}\frac{\Delta t}{\Delta x}(\mathbf{f}(\mathbf{Q}_i) - \mathbf{f}(\mathbf{Q}_{i-1})) \tag{16}$$

and then setting

$$\mathbf{F}^{\mathrm{Ri}}_{i-1/2} = \mathbf{f}(\mathbf{Q}^{\mathrm{Ri}}_{i-1/2}) \tag{17}$$

The FORCE scheme is rather dissipative, as will be seen in the following.

3.2. *The MUSTA approach*

In the MUSTA approach [19, 20], the solution of the Riemann problem at the cell interface is approximated numerically by employing a simple first-order centred method on a local grid. This solution can then be used in (13) or (12).

Here we employ the improved MUSTA scheme of Titarev and Toro [19] using multiple cells on the local grid.

Note that the FORCE flux (14) can be written as

$$\mathbf{F}_{i-1/2} = \mathbf{F}(\mathbf{Q}_{i-1}, \mathbf{Q}_i) = \mathbf{F}(\mathbf{Q}_{\mathrm{L}}, \mathbf{Q}_{\mathrm{R}}) \tag{18}$$

That is, it is only a function of the value to the left and to the right of the cell interface, and it gives rise to a three-point scheme.

In the MUSTA approach, the numerical fluxes $\mathbf{F}_{i-1/2}$ in (13) or (12) are found by transforming the Riemann problem at $x_{i-1/2}$ to a local grid:

$$\frac{\partial \mathbf{Q}}{\partial t} + \frac{\partial \mathbf{F}}{\partial \xi} = \mathbf{0}, \quad \mathbf{Q}(\xi, 0) = \begin{cases} \mathbf{Q}_{i-1} = \mathbf{Q}_{\mathrm{L}} & \text{if } \xi < 0 \\ \mathbf{Q}_i = \mathbf{Q}_{\mathrm{R}} & \text{if } \xi \geqslant 0 \end{cases} \tag{19}$$

Herein, the position $\xi = 0$ corresponds to $x_{i-1/2}$. This local Riemann problem is then solved approximately by employing the FORCE scheme. We index the local grid by n, and, following Titarev and Toro [19], we set $\Delta\xi \equiv \Delta x$. Hence, the FORCE flux $\mathbf{F}(\mathbf{Q}_{n-1}, \mathbf{Q}_n)$ is calculated using the formulae

$$\begin{aligned} \mathbf{F}(\mathbf{Q}_{n-1}, \mathbf{Q}_n) &= \frac{1}{4}\left(\mathbf{F}_{n-1} + 2\mathbf{F}^* + \mathbf{F}_n - \frac{\Delta x}{\Delta t_{\mathrm{loc}}}(\mathbf{Q}_n - \mathbf{Q}_{n-1})\right) \\ \mathbf{F}_{n-1} &= \mathbf{f}(\mathbf{Q}_{n-1}), \quad \mathbf{F}_n = \mathbf{f}(\mathbf{Q}_n) \\ \mathbf{F}^* &= \mathbf{f}(\mathbf{Q}^*), \quad \mathbf{Q}^* = \frac{1}{2}(\mathbf{Q}_{n-1} + \mathbf{Q}_n) - \frac{1}{2}\frac{\Delta t_{\mathrm{loc}}}{\Delta x}(\mathbf{f}(\mathbf{Q}_n) - \mathbf{f}(\mathbf{Q}_{n-1})) \end{aligned} \tag{20}$$

First, the fluxes are computed from (20), where Δt_{loc} is the time-step length calculated using the CFL criterion on the local grid:

$$\Delta t_{\mathrm{loc}} = \frac{C_{\mathrm{loc}} \Delta x}{\max_{1 \leqslant n \leqslant 2N}(\max_{1 \leqslant p \leqslant d} |\lambda_n^p|)} \tag{21}$$

where d is the dimension of the system (1), and the local CFL number, C_{loc}, is a parameter in the method. Next, the local solution is advanced by use of the formula

$$\mathbf{Q}_n^{m+1} - \mathbf{Q}_n^m = -\frac{\Delta t_{\mathrm{loc}}}{\Delta x}(\mathbf{F}_{n+1/2} - \mathbf{F}_{n-1/2}) \tag{22}$$

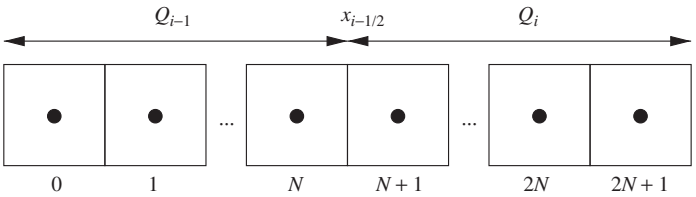

Figure 1. Initial values and cell numbering for the local MUSTA grid.

The local time-stepping is performed a fixed number of times, M, and the local grid has $2N$ cells, in addition to two boundary cells. The initial conditions and the numbering of the local grid are illustrated in Figure 1. The algorithm for the MUSTA flux can be summarized as follows:

1 For each local cell $n = 1, \ldots, 2N$, compute the fluxes on the data from stage m using (20).
2 If $m = M$ then return the FORCE flux $\mathbf{F}^M_{N+1/2}$, else continue.
3 Apply extrapolation boundary conditions; $\mathbf{Q}^m_0 = \mathbf{Q}^m_1$ and $\mathbf{Q}^m_{2N+1} = \mathbf{Q}^m_{2N}$.
4 Update the local solution using (22) for $n = 1, \ldots, 2N$. Repeat from 1.

Thus, the MUSTA flux $\mathbf{F}_{i-1/2}$ to be employed in (12) or (13) is the FORCE flux $\mathbf{F}^M_{N+1/2}$ found on the local grid.

In the above notation, the original FORCE scheme is nearly recovered for $M = 1$ and $2N = 2$. One notable difference, however, is that in the MUSTA approach, the fluxes in (20) are calculated using a *local* CFL criterion, while in the FORCE scheme, the *global* time-step length is used throughout. Here we follow Titarev and Toro [19] and set the local CFL number to $C_{\text{loc}} = 0.9$ for all the calculations.

Note that the cell size of the local grid is without significance, since we are only interested in the solution $\mathbf{F}^M_{N+1/2}$ after a particular number of steps, and not at a particular 'time'.

The MUSTA scheme is constructed to have some of the advantages of upstream schemes. Indeed, for increasing M and N, the MUSTA flux is expected to approach the Godunov flux using the exact Riemann solver [19].

In the following, we will denote the M-stage MUSTA scheme with $2N$ local cells by MUSTA_{M-2N}.

3.3. Higher-order extension

Titarev and Toro [23] suggested to employ weighted essentially non-oscillatory (WENO) schemes in conjunction with MUSTA to produce higher spatial order. Here we propose a different and simpler approach, namely to use a semi-discrete version of the monotone upwind-centred scheme for conservation laws (MUSCL) [24, 25].

In the MUSCL approach, we construct a piecewise linear function using the data $\{\mathbf{Q}_i(t)\}$. Then at the interface $x_{i-1/2}$ we have values on the left and right from the two linear approximations in each of the neighbouring cells. These are denoted by

$$Q^{\text{R}}_{i-1} = Q_{i-1} + \frac{\Delta x}{2}\,\sigma_{i-1} \quad \text{and} \quad Q^{\text{L}}_i = Q_i - \frac{\Delta x}{2}\,\sigma_i \tag{23}$$

where σ_i is a slope calculated using a suitable slope-limiter function. Some are listed by LeVeque [8, Section 9.2]. The *minmod* slope is

$$\sigma_i = \text{minmod}\left(\frac{Q_i - Q_{i-1}}{\Delta x}, \frac{Q_{i+1} - Q_i}{\Delta x}\right) \tag{24}$$

where the minmod function is defined by

$$\text{minmod}(a,b) = \begin{cases} 0 & \text{if } ab \leqslant 0 \\ a & \text{if } |a| < |b| \text{ and } ab > 0 \\ b & \text{if } |a| \geqslant |b| \text{ and } ab > 0 \end{cases} \tag{25}$$

The *monotonized central-difference* (MC) slope [26] is

$$\sigma_i = \text{minmod}\left(\left(\frac{Q_{i+1} - Q_{i-1}}{2\Delta x}\right), 2\left(\frac{Q_i - Q_{i-1}}{\Delta x}\right), 2\left(\frac{Q_{i+1} - Q_i}{\Delta x}\right)\right) \tag{26}$$

We also have the van Leer [27] (see Reference [26]) limiter

$$\sigma_i = \begin{cases} \dfrac{2(Q_i - Q_{i-1})(Q_{i+1} - Q_i)}{(Q_i - Q_{i-1}) + (Q_{i+1} - Q_i)} & \text{if } \text{sgn}(Q_i - Q_{i-1}) = \text{sgn}(Q_{i+1} - Q_i) \\ 0 & \text{otherwise} \end{cases} \tag{27}$$

The slope limiting is applied componentwise to the vector of unknowns. There are different possible choices regarding which variables to use in the slope-limiting procedure, for instance; the composite variables, the primitive variables, or the characteristic variables. The latter would correspond more closely to the scalar case, but would require the diagonalization of the Jacobian matrix, thus defying the purpose of the MUSTA scheme, which is to be simple. Here we use the primitive variables α_g, p, u_g.

When the piecewise linear reconstruction has been performed, the MUSTA flux $\mathbf{F}_{i-1/2} = \mathbf{F}(\mathbf{Q}^R_{i-1}, \mathbf{Q}^L_i)$ is computed as described in the previous subsection. To obtain a second-order solution in time, we employ the semi-discrete formulation (12) in combination with the two-stage second-order strong-stability-preserving (SSP) Runge–Kutta (RK) method (see, e.g. Reference [28]).

With the semi-discrete formulation (12) of the form

$$\frac{\mathrm{d}\mathbf{Q}}{\mathrm{d}t} = \mathscr{L}(\mathbf{Q}) \tag{28}$$

the two-stage second-order SSP-RK method can be written as

$$\begin{aligned} \mathbf{Q}^{(1)} &= \mathbf{Q}^j + \tfrac{1}{2}\Delta t \mathscr{L}(\mathbf{Q}^j) \\ \mathbf{Q}^{j+1} &= \tfrac{1}{2}\mathbf{Q}^j + \tfrac{1}{2}\mathbf{Q}^{(1)} + \tfrac{1}{2}\Delta t \mathscr{L}(\mathbf{Q}^{(1)}) \end{aligned} \tag{29}$$

Herein, $\mathbf{Q}^j$ is the vector of unknowns from time step j, $\mathbf{Q}^{j+1}$ is the sought values at the next time step, while $\mathbf{Q}^{(1)}$ represents intermediate values.

3.4. Comparison with other methods

3.4.1. Reference method. It will be instructive to compare the results produced by the MUSTA scheme to those obtained by using a completely independent numerical method. For that purpose we will employ the wave-propagation (flux-difference splitting) form of Godunov's method presented by LeVeque [8, Chapter 15]. It is a 'high-resolution' method, that is, approaching second order for smooth solutions. The solutions of the Riemann problems at the cell interfaces were found by applying the approximate Riemann solver of Roe [10] to the drift-flux model (1)–(4). The analytical Roe matrix was derived by Flåtten and Munkejord [16].

3.4.2. AUSM schemes. For the current two-phase flow model, an alternative to the Roe scheme denoted as AUSM [29] has been investigated by Evje and Fjelde [13, 14]. Schemes of the AUSM class generally achieve an accuracy comparable to that of the Roe scheme at much lower computational cost. However, they are sometimes prone to introducing numerical oscillations [30], and do not seem to generalize very well to arbitrary systems of conservation laws.

It should nevertheless be noted that for many applications of the drift-flux model, AUSM schemes seem a viable alternative to the MUSTA and Roe schemes considered in this paper, in particular if computational efficiency is of primary importance. We refer to References [13, 14] for details.

4. NUMERICAL SIMULATIONS

In this section, we will analyse the performance of the MUSTA scheme and its MUSCLE extension by conducting basic numerical tests and by running benchmark cases from the literature. Comparisons with the Roe scheme and the FORCE scheme will also be provided. The main aim of the section is to

- Clarify the dependence of the MUSTA scheme on the parameters M and N,
- Explore the performance of the MUSTA scheme for cases where there is a large difference between the largest and the smallest eigenvalue. In particular, we want to demonstrate the importance of the fact that the MUSTA scheme is semi-discrete, which is an essential difference compared to the FORCE scheme.

All the computations in this work have been performed using a local CFL number of $C_{\text{loc}} = 0.9$ in (21).

4.1. Shock tube

This subsection presents calculations of the shock-tube test case of Baudin *et al.* [11]. Baudin *et al.* took the liquid to have a constant density. Here, however, both phases are treated as compressible. The considered horizontal tube is 100 m long, and there is a jump in the initial state at $x = 50$ m. The initial states can be found in Table I, and the equation-of-state parameters are given in Table II. Herein,

$$\rho_k^\circ \equiv c_k^{-2}(p - p_{k,0}) \tag{30}$$

The slip is given by the Zuber–Findlay relation (10) with $K = 1.07$ and $S = 0.2162$.

Table I. Initial states in the shock-tube problem.

Quantity	Symbol (unit)	Left	Right
Gas volume fraction	α_g (–)	0.6	0.55
Pressure	p (kPa)	522.825	803.959
Gas velocity	u_g (m/s)	29.5138	2.5582
Liquid velocity	u_ℓ (m/s)	24.7741	1.7372

Table II. Parameters employed in the shock-tube problem.

	c_k (m/s)	ρ_k° (kg/m^3)
Gas (g)	300	0
Liquid (ℓ)	1000	999.916

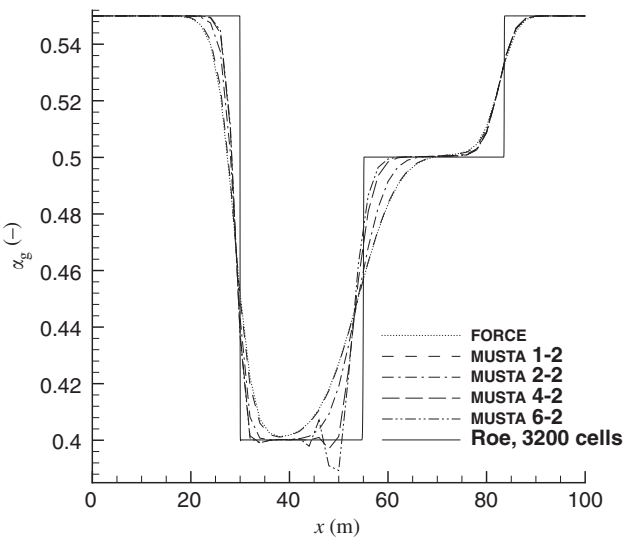

Figure 2. Gas volume fraction for the shock-tube test case. Dependency on the number of stages, M, for the MUSTA$_{M-2}$ scheme.

First, we will investigate the dependence upon the parameters M and N, that is, the number of stages and the number of local cells. Thereafter, the convergence of the basic MUSTA scheme and the MUSCL-MUSTA scheme will be tested.

4.1.1. Effect of number of stages and local cells. Figure 2 shows the volume fraction calculated on a 50-cell grid using a CFL number of $C = 0.9$ in (11). The results are plotted at $t = 0.5$ s. The reference solution was obtained on a 3200-cell grid with the Roe method employing the MC limiter. The data in the figure have been calculated using two local cells, or $N = 1$, and the number of local time steps, M, has been varied. The difference between MUSTA$_{1-2}$ and FORCE is that in FORCE, only the global time-step length is employed, while

MUSTA$_{1-2}$ uses a local CFL criterion for the calculation of the intercell fluxes. This is also the difference between the MUSTA$_{M-2}$ scheme discussed here and the two-cell MUSTA scheme proposed by Toro [20]. For the present case, there is only a small difference between the results produced with MUSTA$_{1-2}$ and those from FORCE.

When M is increased from 1 to 2, the performance of the scheme is clearly improved. However, as M is further increased, the monotonicity is lost and grave oscillations occur. This is in contrast to what was reported by Toro [20] for the Euler equations. There, satisfactory results were shown for the four-stage two-cell MUSTA scheme.

Figure 3 shows why MUSTA cannot be expected to give good results in general when the number of stages, M, is greater than the number of cells, N, on each side of the discontinuity. The figure displays the gas velocity as calculated in the local MUSTA procedure for a varying number of local cells, $2N$. The right and left states are the same as in the shock-tube test case, and the results are shown after $M=4$ local time steps. Figure 3(a) shows the whole domain, while Figure 3(b) highlights the results for the middle cells. It is the values from these cells that are used to compute the intercell flux. As can be seen in Figure 3(a), the calculation domain grows as the number of local cells is increased.

Figure 3(b) shows a clear discrepancy between the values obtained with $N=1$ (two local cells) and $N=2$ (four local cells). On the left-hand side, a small difference can also be seen between the values calculated for $N=2$ and 3 (six local cells). The results for $N=3$ and 4 are identical in the two middle cells.

Due to the CFL criterion, a wave can travel one cell per time step. For $N=2$, that is, with two internal cells on each side of the Riemann discontinuity, a wave may travel to the boundary, be (partially) reflected, and return to the origin in four time steps. On the other hand, for $N=3$, the wave has no longer the time to return. This is why there is a difference between the $N=2$ and 3 results, while the results for $N=3$ and 4 are equal.

As a conclusion, we may say that to be certain that boundary effects do not interfere in the calculation of the MUSTA flux, one must choose $M<2N$. However, the results in Figure 3 indicate that $M=2N$ may also give good results.

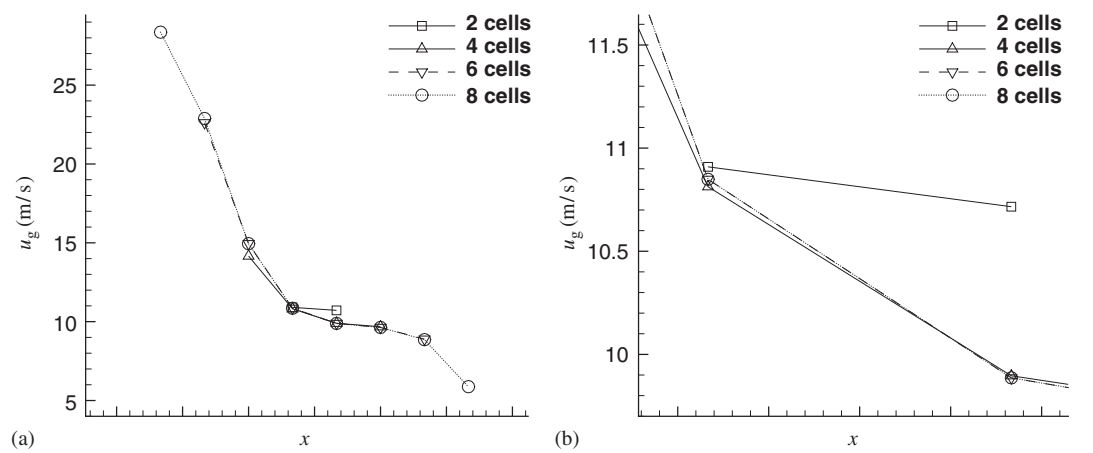

Figure 3. Gas velocity on the local MUSTA grid for the shock tube. Results after four local MUSTA time steps for varying number of local cells: (a) whole domain; and (b) close-up on $x_{N+1/2}$.

The bad results for $M > 2N$ may be due to the rather simplified boundary treatment in the local MUSTA procedure, which has as a consequence that when N is set too low, information disappears from the calculation domain in an unmotivated way. This is because every variable at the boundaries is found from the inner domain by zeroth-order extrapolation. Hence, the boundary conditions are not set according to the number of positive and negative characteristics, as they ought to be. However, instead of enforcing a rigorous boundary treatment in the local MUSTA procedure, it is adequate simply to choose a sufficiently large local grid.

The effect of the simultaneous increase of the number of stages, M, and the number of local cells, $2N$, is shown in Figure 4. As can be seen from the plot, it is primarily the resolution of the contact discontinuity that is improved for an increased number of stages. However, the difference between four and eight stages is small. In the graph we have also plotted data obtained with the first-order Roe method on the same grid and using the same CFL number. It is noticeable that the MUSTA results approach those of the Roe scheme when the number of stages is increased. For eight stages, the results obtained with the MUSTA scheme are very similar to those calculated using the Roe method.

4.1.2. Some comparisons with the FORCE scheme. Figure 5 shows volume-fraction profiles for computations performed on a 50-cell grid using various time-step lengths (CFL numbers). Results for MUSTA_{1-2} are displayed in Figure 5(a), while Figure 5(b) gives profiles for the FORCE scheme. It can be seen that the FORCE scheme becomes increasingly diffusive as the time-step length is decreased. This is due to the $\Delta x/\Delta t$ term of the Lax–Friedrichs flux, and it reflects the fact that the FORCE scheme has no semi-discrete form. The results of the MUSTA_{1-2} scheme, on the other hand, converge for decreasing time-step lengths, and there is only a small difference between the results for $C = 0.1$ and those for $C = 0.01$. This behaviour

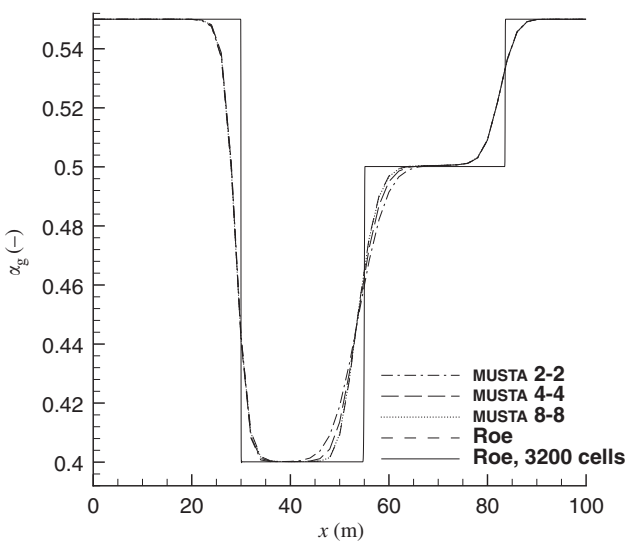

Figure 4. Gas volume fraction for the shock-tube test case. Effect of varying number of stages and local cells in the MUSTA_{M-2N} scheme.

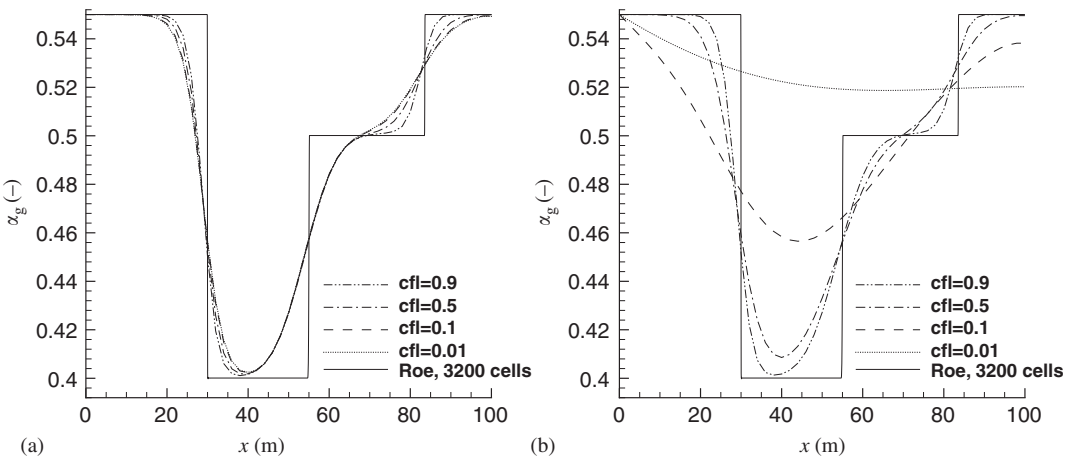

Figure 5. Gas volume fraction for the shock-tube test case. Comparison of the MUSTA_{1-2} scheme and the FORCE scheme for varying CFL number (time-step length). 50 grid cells: (a) MUSTA_{1-2}; and (b) FORCE.

is expected from a semi-discrete scheme, even though it does not prove in itself that the scheme is semi-discrete.

There are two main reasons for the differences between MUSTA and FORCE. In MUSTA, as opposed to in FORCE, the intercell fluxes are calculated using a *local* CFL criterion. Furthermore, in MUSTA, when more local time steps are taken, the neighbouring global cells do not interfere in the calculation. In FORCE, when the global grid is refined, more time steps are performed due to the CFL criterion. Therefore, more neighbouring cells are affected, since information propagates one cell per time step.

4.1.3. Convergence of basic scheme. Figure 6 displays data obtained on various grids with the MUSTA_{4-4} scheme, that is, the four-stage MUSTA scheme with four local cells. The CFL number was $C = 0.9$. As can be seen, the results are non-oscillatory, and both the shocks and the contact discontinuity are quite sharply resolved. In fact, the results are similar to those of the first-order Roe scheme, except that the contact discontinuity is slightly more smeared.

4.1.4. Higher-order scheme. Figure 7 shows a comparison between the first-order MUSTA_{4-4} scheme and its MUSCL extension. The employed grid had 50 cells and the CFL number was $C = 0.5$. Results obtained with the MC-limited Roe method are also shown for comparison. Employing MUSCL-MUSTA_{4-4} with the minmod limiter gave a sharper resolution of both the shocks and the contact discontinuity, compared to the first-order MUSTA_{4-4} scheme. However, as can be observed, the Roe-MC scheme gave a still better resolution, particularly for the right-hand-side shock. Unfortunately, using less-diffusive limiters than the minmod limiter gave oscillations with the MUSCL-MUSTA_{4-4} scheme. This is shown in the figure for the van Leer limiter. Henceforth, we therefore only consider the minmod limiter.

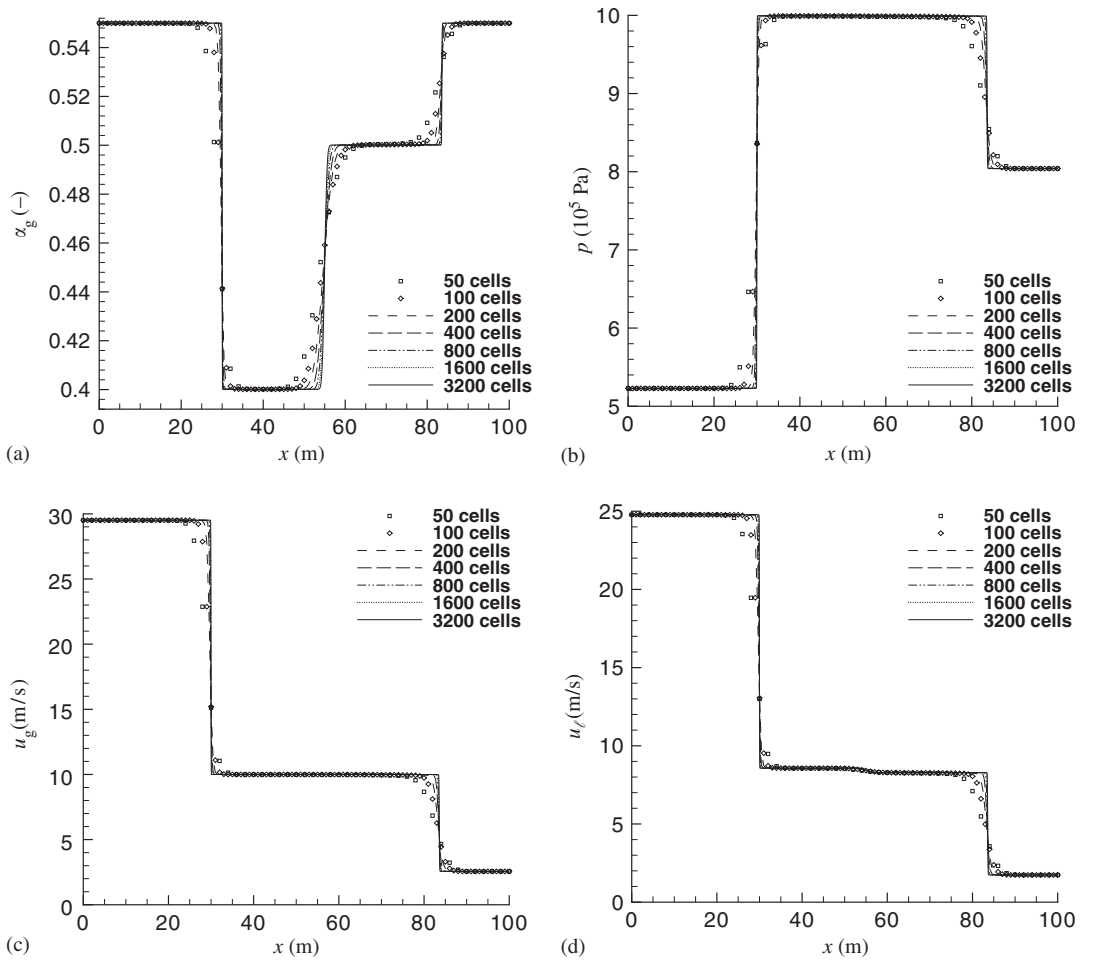

Figure 6. Shock tube. Convergence of the MUSTA$_{4-4}$ scheme: (a) gas volume fraction; (b) pressure; (c) gas velocity; and (d) liquid velocity.

The convergence for MUSCL-MUSTA$_{4-4}$ using the minmod limiter is displayed in Figure 8 for $C = 0.5$. The results are non-oscillatory, and both the shocks and the discontinuity are well resolved. Nevertheless, the MC-limited Roe scheme gave a sharper resolution [16].

4.1.5. Computational cost. A comparison of the CPU-time consumption of different MUSTA$_{M-2N}$ schemes and the Roe scheme is shown in Table III. The calculations were run using a CFL number of 0.9. Data are only shown for a 800-cell grid, since no grid dependency was detected. The second column shows the CPU time of the MUSTA$_{M-2N}$ schemes divided by that of the first-order Roe scheme, while the third column shows the figures for the MUSCL-MUSTA$_{M-2N}$ schemes employing the minmod limiter and the Roe scheme using the MC limiter.

The table shows that as the number of local time steps, M, and local cells, $2N$, are increased, the computational cost of the MUSTA schemes strongly grows. As noted in the

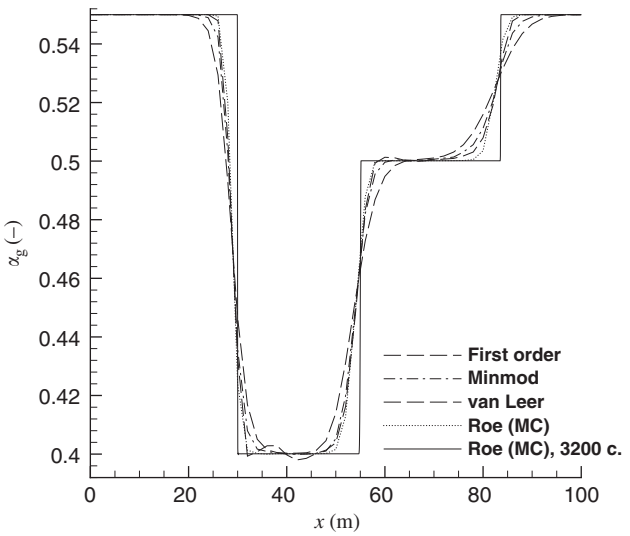

Figure 7. Gas volume fraction for the shock-tube test case. Comparison of the first-order and the MUSCL-MUSTA$_{4-4}$ scheme with different limiter functions on a 50-cell grid.

previous subsections, the MUSTA scheme comes quite close to the accuracy of the Roe scheme for $M = 4$ and $2N = 4$. Therefore, it is most relevant to compare the CPU-time consumption of the (MUSCL-) MUSTA$_{4-4}$ scheme and that of the Roe method.

While care has been taken during the implementation of both types of schemes not to waste too much CPU time, optimizations are undoubtedly possible. Particularly for MUSCL-MUSTA, there are some degrees of freedom regarding the implementation. Therefore, instead of declaring a 'CPU-time winner', one may only conclude that

- the CPU-time consumption of the MUSTA$_{4-4}$ scheme and the Roe scheme are of the same order of magnitude, and
- the CPU-time consumption of MUSCL-MUSTA$_{M-2N}$ is relatively larger than that of MUSTA$_{M-2N}$.

It is perhaps surprising that the centred scheme MUSTA$_{4-4}$ is not computationally much cheaper than the Roe scheme for a given grid size and time-step length. The reason is that the numerical diagonalization and matrix manipulations performed in the Roe scheme are roughly balanced by the extra computations carried out on the local MUSTA grid. This includes extra evaluations of the equation of state and the slip relation.

The second-order Roe scheme is relatively cheaper than the MUSCL-MUSTA$_{4-4}$ scheme, since in the Roe scheme, the high-resolution terms are already mostly calculated during the diagonalization of the Jacobian matrix. In MUSCL-MUSTA, on the other hand, the piecewise reconstruction of the data comes fully in addition to the calculations done in the basic scheme.

4.2. *Pure rarefaction*

We now study the pure-rarefaction problem of Baudin *et al.* [11], where the initial values are given in Table IV, and the equation-of-state parameters are reported in Table V. In the present problem, the no-slip law is used, that is, $\Phi \equiv 0$.

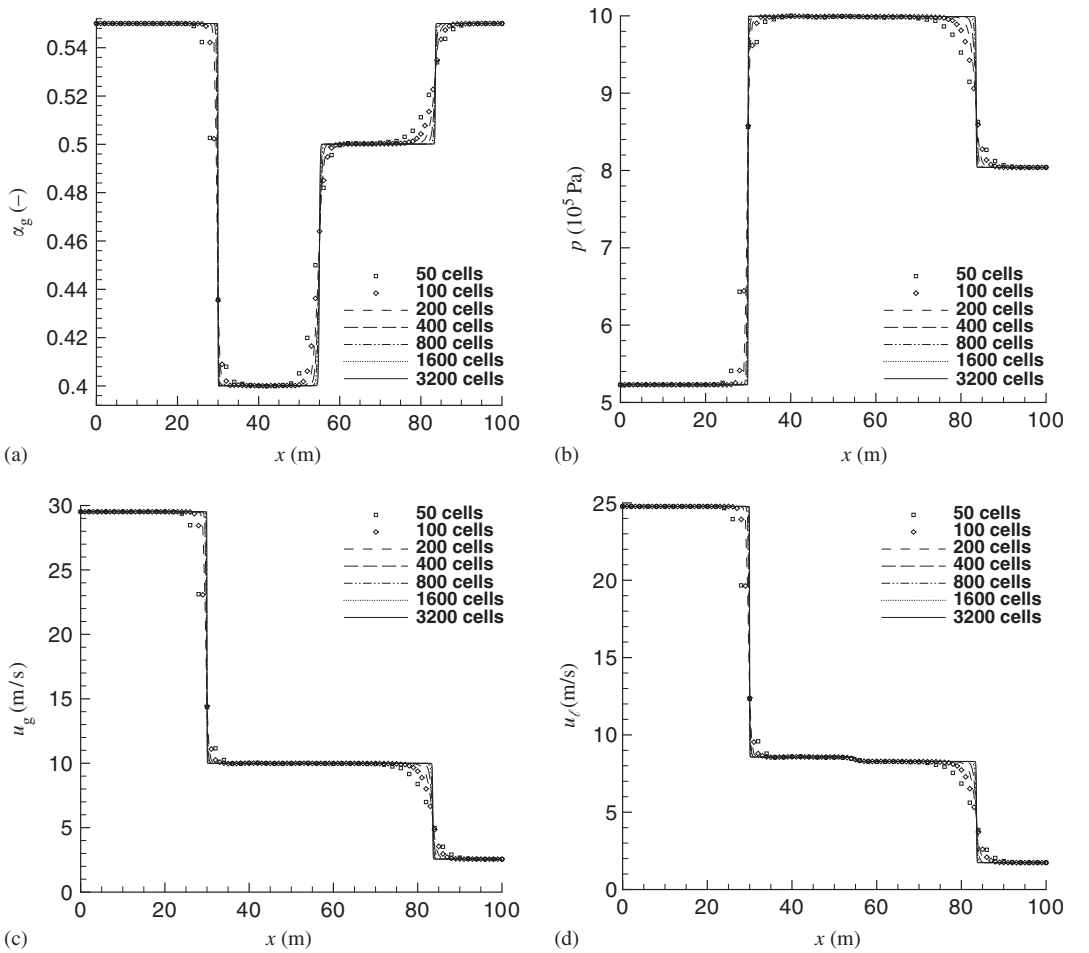

Figure 8. Shock tube. Convergence of the MUSCL-MUSTA$_{4-4}$ scheme using the minmod limiter: (a) gas volume fraction; (b) pressure; (c) gas velocity; and (d) liquid velocity.

Table III. Shock-tube test case. Comparison of CPU-time consumption.

$M-2N$	MUSTA$_{M-2N}$/Roe	M-MUSTA$_{M-2N}$/Roe-MC
$1-2$	0.19	0.40
$2-2$	0.32	0.67
$4-4$	0.78	1.58
$8-8$	2.28	4.65

Pressure profiles at $t=0.8$ s are presented in Figure 9 for various grid sizes. The employed CFL number was $C=0.5$. Figure 9(a) shows the results for the basic four-stage MUSTA scheme with four local cells. Data for the first-order Roe scheme on a 50-cell grid are shown for comparison, and it can be observed that the results are very similar. As can be seen from

Table IV. Initial states in the pure-rarefaction test problem.

Quantity	Symbol (unit)	Left	Right
Gas volume fraction	α_g (–)	0.6	0.68
Pressure	p (MPa)	1.66667	1.17647
Gas velocity	u_g (m/s)	34.4233	50.0
Liquid velocity	u_ℓ (m/s)	34.4233	50.0

Table V. Parameters employed in the rarefaction test problems.

	c_k (m/s)	ρ_k° (kg/m^3)
Gas (g)	100	0
Liquid (ℓ)	1000	998.924

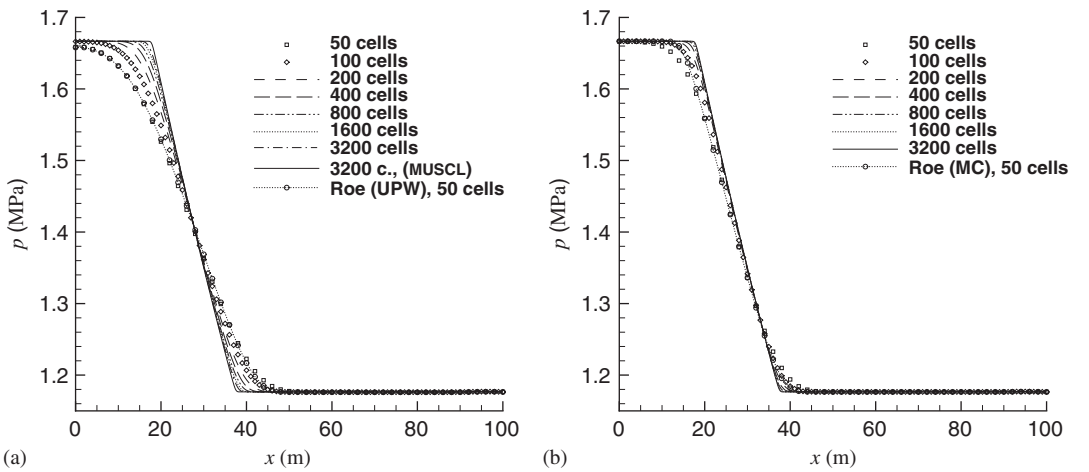

Figure 9. Pressure for the pure-rarefaction test problem. Convergence of the MUSTA$_{4-4}$ scheme and its MUSCL extension: (a) basic scheme (first-order); and (b) MUSCL with minmod limiter.

Figure 9(b), the MUSCL extension using the minmod limiter represents an improvement over the standard MUSTA scheme. However, the resolution is not quite as good as that obtained using the MC-limited Roe scheme.

4.3. Transonic rarefaction

Transonic rarefactions, that is, when an eigenvalue λ^p is negative to the left of the pth wave, and positive to the right, are not automatically handled by the Roe scheme if an entropy fix is not implemented. It is therefore interesting to compare the performance of the Roe and MUSTA schemes in such a case.

A transonic rarefaction (and some other waves) can be produced by decreasing the pressure and increasing the velocities on the right-hand side of the pure-rarefaction test case. The initial states are listed in Table VI, and the equation-of-state parameters are given in Table V.

Table VI. Initial states in the transonic-rarefaction test problem.

Quantity	Symbol (unit)	Left	Right
Gas volume fraction	α_g (–)	0.6	0.68
Pressure	p (MPa)	1.66667	0.7
Gas velocity	u_g (m/s)	34.4233	70.0
Liquid velocity	u_ℓ (m/s)	34.4233	70.0

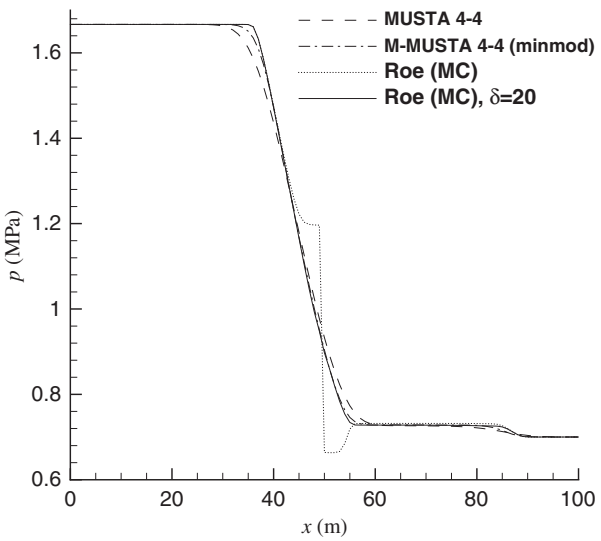

Figure 10. Pressure for the transonic-rarefaction problem. Comparison of the MUSTA$_{4-4}$ scheme, the MUSCL-MUSTA$_{4-4}$ scheme using the minmod limiter, the MC-Roe scheme, and the MC-Roe scheme employing Harten's entropy fix with $\delta = 20$. 100 grid cells.

The plot in Figure 10 shows pressure profiles obtained after $t = 0.3$ s on a 100-cell grid, using a CFL number of $C = 0.5$. The MC-limited Roe scheme produced a rarefaction shock, something which is unphysical. As shown, this can be remedied by employing the entropy fix of Harten [31]. Here we took the parameter $\delta = 20$[‖]. It can also be seen from the figure that both the MUSTA$_{4-4}$ scheme and the MUSCL-MUSTA$_{4-4}$ scheme using the minmod limiter gave physically plausible solutions.

4.4. Static discontinuity

We next consider a static discontinuity. This test case clearly reveals differences between upwind and central schemes. Upwind schemes are known to preserve a static discontinuity, whereas central schemes will gradually smear it out.

[‖]Written in the notation of LeVeque [8, Section 15.3]. In the notation of Harten, this corresponds to $\varepsilon = 10$.

Table VII. Initial states in the static-discontinuity test problem.

Quantity	Symbol (unit)	Left	Right
Gas volume fraction	α_g (–)	0.2	0.8
Pressure	p (kPa)	100	100
Gas velocity	u_g (m/s)	0	0
Liquid velocity	u_ℓ (m/s)	0	0

Table VIII. Parameters employed in the static-discontinuity test problem.

	c_k (m/s)	ρ_k° (kg/m^3)
Gas (g)	$\sqrt{10^5}$	0
Liquid (ℓ)	1000	999.9

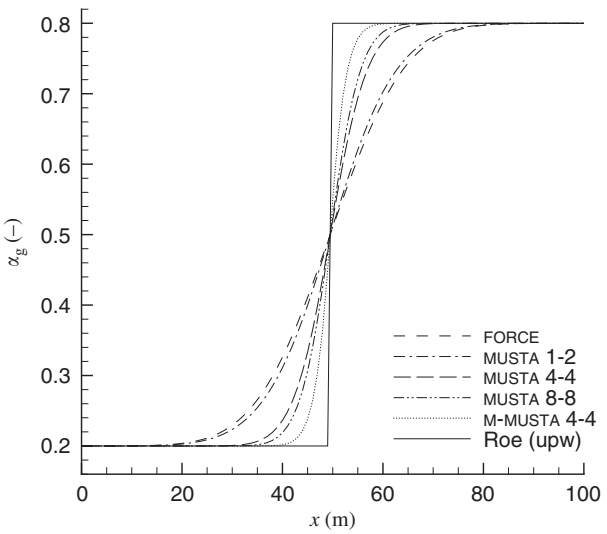

Figure 11. Gas volume fraction for the static discontinuity. Comparison of the FORCE scheme, various MUSTA$_{M-2N}$ schemes and the MUSCL-MUSTA$_{4-4}$ scheme with the minmod limiter. 100 grid cells.

This test consists of a discontinuity in the volume fraction, while the other variables are uniform. The velocities are zero. The initial states are given in Table VII, and Table VIII shows the parameters employed in the equation of state.

Figure 11 shows gas-volume-fraction profiles after $t = 10$ s calculated on a 100-cell grid using $C = 0.9$. As expected, the performance of the MUSTA schemes improved as the number of stages was increased. The curve labelled M-MUSTA is for the MUSCL extension using the minmod limiter, and it shows that the MUSCL approach provided some improvement. The figure also shows that the FORCE scheme is the most diffusive, whereas the first-order Roe scheme perfectly preserves the discontinuity.

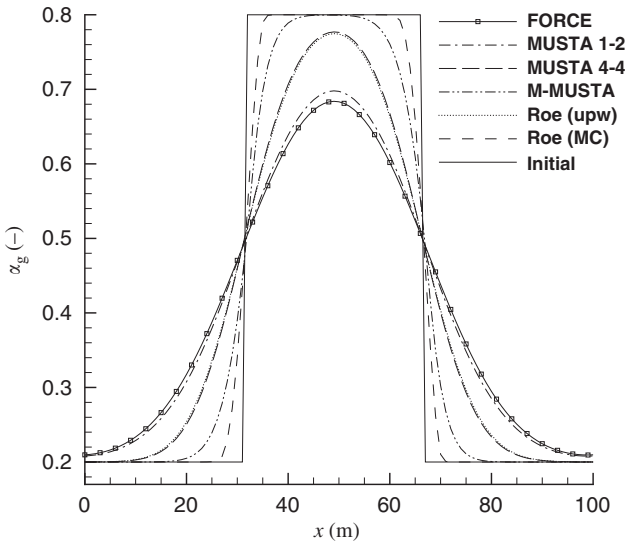

Figure 12. Gas volume fraction for the moving discontinuity. Comparison of the FORCE scheme, MUSTA_{M-2N} schemes and the MUSCL-MUSTA_{4-4} scheme with the minmod limiter. The first-order (upwind) Roe scheme and the MC-limited Roe scheme are also shown. 100 grid cells.

It should be noted that the MUSTA scheme keeps smearing the discontinuity even when both the local and global CFL numbers are set equal to 1.

4.5. *Moving discontinuity*

Now we let the discontinuity move. The initial conditions are similar to those of the static-discontinuity case, except that both phases have a velocity of $u = 10\,\text{m/s}$. There is no slip between the phases. Instead of a single jump in the volume fraction, there is now a 'hat'. Periodic boundary conditions are employed.

Figure 12 displays volume-fraction profiles after $t = 10\,\text{s}$, that is, the volume fraction 'hat' has traversed the calculation domain once. As for the static-discontinuity case, the grid had 100 cells and the CFL number was $C = 0.9$. The initial profile is plotted for reference. For this case, the first-order Roe scheme (labelled 'upw') has no particular advantage compared to the MUSTA_{4-4} scheme. Results for MUSTA_{8-8} are not shown, since they were very similar to those of MUSTA_{4-4}. The Roe scheme employing the MC limiter gave the best resolution, while the MUSCL-MUSTA_{4-4} scheme lay in between that and the first-order schemes. Nevertheless, the most interesting point is that the performance of the MUSTA_{4-4} scheme is rather close to that of the Roe scheme.

4.6. *Pipe-flow problem*

We finally turn to the pipe-flow problem, which was introduced as Example 4 by Evje and Fjelde [14]. This is a demanding test, particularly regarding mass transport, and it includes such

Table IX. Parameters employed in the pipe-flow problem.

	c_k (m/s)	ρ_k° (kg/m^3)
Gas (g)	$\sqrt{10^5}$	0
Liquid (ℓ)	1000	999.9

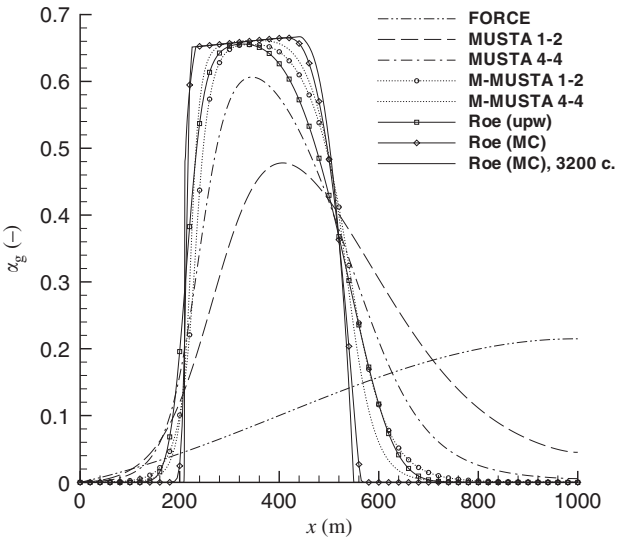

Figure 13. Gas volume fraction for the pipe-flow test problem. Comparison of the FORCE scheme, MUSTA$_{M-2N}$ schemes and the MUSCL-MUSTA$_{4-4}$ scheme with the minmod limiter. The first-order (upwind) Roe scheme and the MC-limited Roe scheme are also shown. 200 grid cells.

challenges as a more complex, non-linear slip relation and near-single-phase flow. Moreover, the near-single-phase flow causes a large difference between the eigenvalues.

The equation-of-state parameters are given by Table IX. In the slip relation (10), $K = 1$ is constant, but S is now a non-linear function of the volume fraction:

$$S = S(\alpha_g) = \tfrac{1}{2}\sqrt{1 - \alpha_g} \tag{31}$$

Further, a wall-friction model is included:

$$F_w = \frac{32 u_m \eta_m}{d^2} \tag{32}$$

where u_m is the mixture velocity,

$$u_m = \alpha_g u_g + \alpha_\ell u_\ell \tag{33}$$

and the dynamic mixture viscosity, η_m, is taken to be

$$\eta_m = \alpha_g \eta_g + \alpha_\ell \eta_\ell \tag{34}$$

with $\eta_g = 5 \times 10^{-6}$ Pa s and $\eta_\ell = 5 \times 10^{-2}$ Pa s.

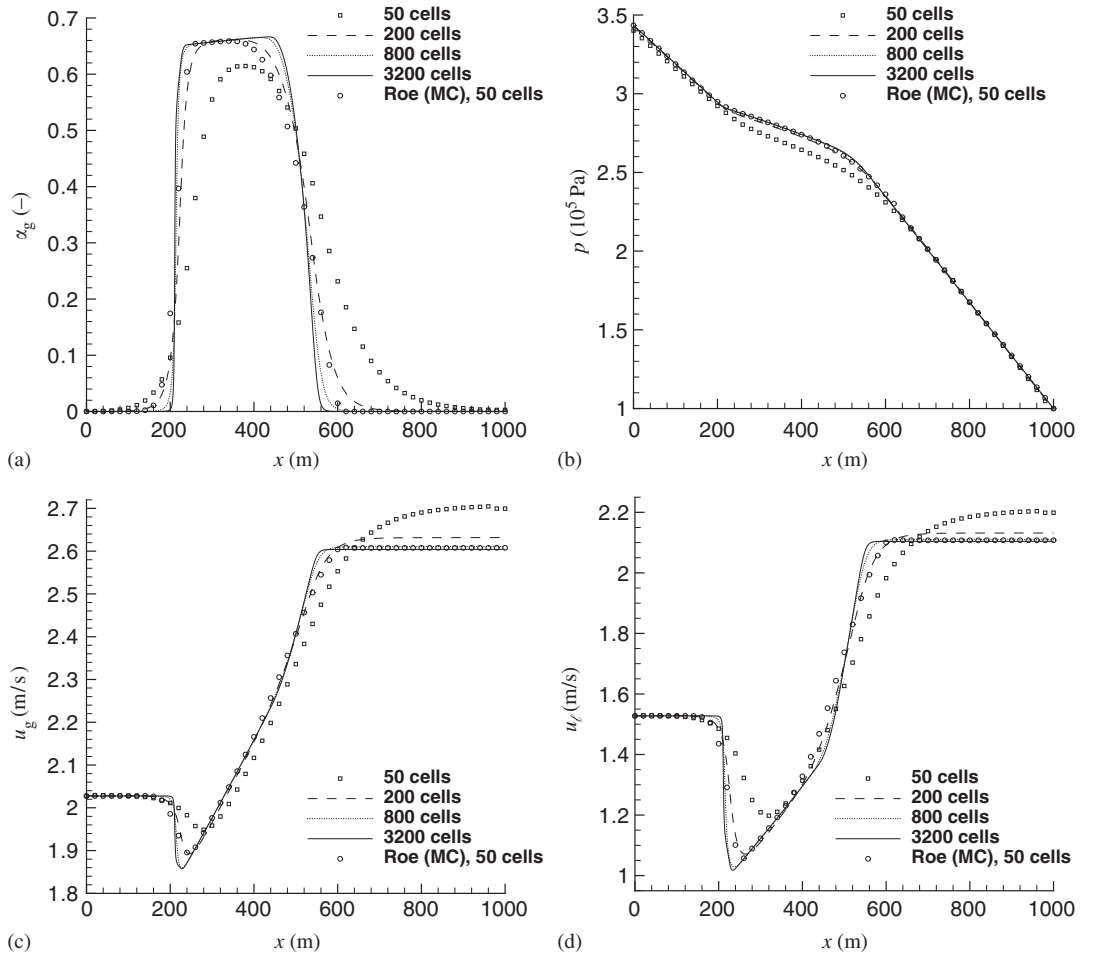

Figure 14. Pipe-flow test problem. Convergence of the MUSCL-MUSTA4−4 scheme using the minmod limiter: (a) gas volume fraction; (b) pressure; (c) gas velocity; and (d) liquid velocity.

The problem consists of a horizontal pipe of length $l = 1000$ m and inner diameter $d = 0.1$ m. Initially, it is filled with stagnant, almost-pure liquid, with $\alpha_g = 1 \times 10^{-5}$. Furthermore, the details of the simulation are specified as follows:

- The simulation lasts for 175 s.
- Between $t = 0$ and 10 s, the gas and liquid inlet mass-flow rates are linearly increased from 0 to 0.08 kg/s and 12.0 kg/s, respectively.
- From $t = 10$ to 175 s, the inlet liquid mass-flow rate is kept constant.
- The inlet gas mass-flow rate is kept constant between $t = 10$ and 50 s.
- Between $t = 50$ and 70 s, the inlet gas mass-flow rate is linearly decreased from 0.08 to 1×10^{-8} kg/s, after which it is kept constant.
- At the outlet, the pressure is kept constant at $p = 1 \times 10^5$ Pa.

A comparison of different MUSTA variants, the FORCE scheme and the Roe scheme is given in Figure 13. The computations were performed on a 200-cell grid using $C = 0.5$. The solution obtained with the MC-limited Roe scheme on a fine grid is shown for reference. First, it is obvious that the FORCE scheme is useless for this kind of calculation due to its smearing of volume-fraction waves. The time-steps calculated according to (11) became very small because of the transition to single-phase flow, and we observe a behaviour which is similar to the one seen in Figure 5. Next, it is somewhat surprising that already MUSTA_{1-2} provided a noticeable improvement, the only difference between the two schemes being that the latter employs a local CFL number of 0.9 in the calculation of the intercell fluxes. For an increasing number of stages, the MUSTA scheme gave better results, but even MUSTA_{8-8} did not quite attain the volume-fraction profile of the first-order Roe scheme. Similar to what has been seen in the previous test problems, MUSCL-MUSTA_{4-4} with the minmod limiter gave quite good results, but not as sharp as those of the Roe scheme using the MC limiter.

It is interesting that the difference between the volume-fraction profile of MUSTA_{1-2} and that of MUSCL-MUSTA_{1-2} is significantly larger than the difference between MUSTA_{4-4} and MUSCL-MUSTA_{4-4}. Furthermore, the volume-fraction profile of MUSCL-MUSTA_{1-2} is not far from that of MUSCL-MUSTA_{4-4}. Hence, the former scheme may be of interest for practical calculations, since it is less CPU-intensive.

Calculations performed with the MUSCL-MUSTA_{4-4} scheme for various grids using $C = 0.5$ are plotted in Figure 14. The results are non-oscillatory, and it can be observed that the near-single-phase flow is handled well. The results are comparable to those presented for the second-order AUSMD scheme in Evje and Fjelde [14]. Still, the resolution is not quite as good as the one obtained using the MC-limited Roe method.

5. DISCUSSION

The multi-stage (MUSTA) centred scheme has been analysed for the drift-flux model. In this scheme, an approximate solution to the Riemann problem at the cell interfaces is found by running the first-order centred (FORCE) scheme a given number of time steps (M) on a $2N$-cell local grid. The scheme is of special interest, since it uses no explicit information of the eigenstructure of the model, while giving a significantly improved solution compared to the FORCE scheme. Still, the scheme is dependent on an estimate of the maximum eigenvalue to be able to employ the CFL criterion.

To avoid interference from the boundaries in the local MUSTA procedure, it is necessary to choose $M < 2N$. However, in the present computations, $M = 2N$ also gave good results. Choosing $M > 2N$ may yield oscillatory solutions and should be avoided.

The four-stage MUSTA scheme with four local cells ($M = 4$ and $N = 2$) gave results quite close to those of the first-order Roe scheme. In contrast to the Roe scheme, however, MUSTA did not preserve a static discontinuity. On the other hand, MUSTA handled a transonic rarefaction without producing an entropy-condition violation.

To achieve higher order in time and space, we have proposed to use the MUSTA flux in a semi-discrete MUSCL formulation. The resulting MUSCL-MUSTA scheme employing the minmod limiter produced improved and non-oscillatory results. A pipe-flow problem emphasizing volume-fraction waves and near-single-phase flow was well resolved, albeit with a less sharp resolution than the one obtained with the MC-limited Roe scheme. Unfortunately, MUSCL-MUSTA

could not in general be used with less-diffusive limiters, since they produced oscillatory solutions for the tested shock tube.

Provided the number of stages is chosen within the bounds described above, the MUSTA scheme possesses robustness properties comparable to those of the Roe scheme. In particular, it generally resolves shock fronts in a non-oscillatory manner and seems to be able to handle the transition to single-phase flow while preserving positivity of volume fractions.

Since its computational cost increases quite quickly with the number of stages and local cells, the main advantage of the MUSTA scheme is its simplicity.

6. CONCLUSIONS

- The MUSTA scheme has been successfully applied to the drift-flux model, which is relatively complicated compared to the Euler equations. In particular, the scheme worked well for a test problem with a large gap between the eigenvalues.
- The results of the basic MUSTA scheme approached those of the first-order Roe scheme. However, the MUSCL-MUSTA scheme did not quite attain the results of the second-order Roe scheme based on wave decomposition. This is mainly since it was necessary to employ a more-diffusive limiter function in MUSCL-MUSTA.
- The computational cost of the MUSTA scheme is comparable to that of the Roe scheme.
- MUSTA seems to be an appropriate choice of numerical scheme if
  1. It is desired to employ closure laws for which the Roe scheme is not valid, e.g. closure laws including additional terms on differential form.
  2. One wishes to avoid programming the numerical diagonalization performed in the Roe scheme.
  3. One wants to avoid possible problems due to transonic rarefactions.

APPENDIX A: APPROXIMATE EIGENVALUES

In this work, we employed the approximate eigenvalues derived by Evje and Flåtten [5] using a perturbation technique under the assumption that the slip relation Φ satisfies the differential equation

$$\alpha_\ell \left(\frac{\partial \Phi}{\partial \alpha_\ell} \right)_p + \Phi = 0 \tag{A1}$$

In the following, we employ the definitions

$$m_k = \alpha_k \rho_k \tag{A2}$$

$$\mu_k = \left(\frac{\partial \Phi}{\partial m_k} \right)_{m_\mathrm{f}, u_\mathrm{f}} \qquad k \neq f \tag{A3}$$

$$\zeta = \left(\frac{\partial u_\ell}{\partial u_\mathrm{g}} \right)_{m_\mathrm{g}, m_\ell} \tag{A4}$$

$$\varrho = m_{\mathrm{g}} + \zeta m_{\ell} \tag{A5}$$

$$\kappa = \frac{1}{(\partial \rho_{\mathrm{g}}/\partial p)\alpha_{\mathrm{g}}\rho_{\ell} + (\partial \rho_{\ell}/\partial p)\alpha_{\ell}\rho_{\mathrm{g}}} \tag{A6}$$

With the perturbation parameter

$$\varepsilon = \frac{u_{\mathrm{g}} - u_{\ell}}{\sqrt{\kappa\varrho(\alpha_{\mathrm{g}} - \zeta\alpha_{\ell})}} \tag{A7}$$

the eigenvalue corresponding to the material wave was found to be

$$\lambda_{\mathrm{m}} = u_{\mathrm{g}} - \frac{\alpha_{\mathrm{g}}\alpha_{\ell}}{\alpha_{\mathrm{g}} + \zeta\alpha_{\ell}}\mu_{\mathrm{g}}\frac{(u_{\mathrm{g}} - u_{\ell})^2}{\kappa} + \mathcal{O}(\varepsilon^3) \tag{A8}$$

and the eigenvalues corresponding to the sonic waves were calculated as

$$\lambda_p = u_p \pm c_{\mathrm{m}} \tag{A9}$$

where

$$u_p = \frac{m_{\mathrm{g}}u_{\mathrm{g}} + \zeta m_{\ell}u_{\ell}}{m_{\mathrm{g}} + \zeta m_{\ell}} + \alpha_{\ell}m_{\mathrm{g}}\mu_{\mathrm{g}}\frac{\rho_{\ell} - \rho_{\mathrm{g}}}{2\varrho} + \frac{\alpha_{\mathrm{g}}\alpha_{\ell}}{\alpha_{\mathrm{g}} + \zeta\alpha_{\ell}}\mu_{\mathrm{g}}\frac{(u_{\mathrm{g}} - u_{\ell})^2}{2\kappa} + \mathcal{O}(\varepsilon^3) \tag{A10}$$

and the mixture sonic velocity is

$$c_{\mathrm{m}} = \frac{1}{2}\psi_1\psi_3 + \frac{\psi_{12}}{\psi_{13}}\frac{\rho_{\ell}}{\varrho}\left[2 - \zeta\alpha_{\ell}\left(\frac{\rho_{\ell} - \rho_{\mathrm{g}}}{\varrho}\right)\right](u_{\mathrm{g}} - u_{\ell}) + \mathcal{O}(\varepsilon^2) \tag{A11}$$

with

$$\begin{aligned}
\psi_1 &= \sqrt{\kappa\varrho(\alpha_{\mathrm{g}} + \zeta\alpha_{\ell})} \\
\psi_2 &= \frac{\alpha_{\ell}m_{\mathrm{g}}}{\psi_1}\mu_{\mathrm{g}} \\
\psi_3 &= \sqrt{\psi_2^2\left(\frac{\rho_{\ell} - \rho_{\mathrm{g}}}{\varrho}\right)^2 + 4\frac{\rho_{\ell}\rho_{\mathrm{g}}}{\varrho^2}}
\end{aligned} \tag{A12}$$

ACKNOWLEDGEMENTS

We thank the Research Council of Norway for financial support through a personal Ph.D. grant (first author), and through the BeMatA programme (second and third authors).

We are grateful to Jens A. Melheim at NTNU, who has commented the manuscript and provided useful suggestions. Thanks are also due to the referees for their constructive remarks.

REFERENCES

1. Drew DA, Passman SL. *Theory of Multicomponent Fluids*, *Applied Mathematical Sciences*, vol. 135. Springer: New York, 1999. ISBN 0-387-98380-5.
2. Bendiksen KH. An experimental investigation of the motion of long bubbles in inclined tubes. *International Journal of Multiphase Flow* 1984; **10**(4):467–483.

3. Bouré JA. Wave phenomena and one-dimensional two-phase flow models—part I: kinematic waves; experimental results; theory. *Multiphase Science and Technology* 1997; **9**(1):1–35.
4. França F, Lahey Jr RT. The use of drift-flux techniques for the analysis of horizontal two-phase flows. *International Journal of Multiphase Flow* 1992; **18**(6):787–801.
5. Evje S, Flåtten T. On the wave structure of two-phase flow models. Preprint available from http://www.rf.no/Internet/petroleum.nsf/p/205, 2005, submitted.
6. Pauchon CL, Dhulesia H, Cirlot GB, Fabre J. TACITE: a transient tool for multiphase pipeline and well simulation. *Proceedings—SPE Annual Technical Conference and Exhibition*, Π Production Operations and Engineering, vol. 2. Society of Petroleum Engineers, New Orleans, Louisiana, U.S.A., SPE 28545. 311–326.
7. Romate JE. An approximate Riemann solver for a two-phase flow model with numerically given slip relation. *Computers and Fluids* 1998; **27**(4):455–477.
8. LeVeque RJ. *Finite Volume Methods for Hyperbolic Problems*. Cambridge University Press: Cambridge, U.K., 2002. ISBN 0-521-00924-3.
9. Toro EF. *Riemann Solvers and Numerical Methods for Fluid Dynamics* (2nd edn). Springer: Berlin, 1999. ISBN 3-540-65966-8.
10. Roe PL. Approximate Riemann solvers, parameter vectors, and difference schemes. *Journal of Computational Physics* 1981; **43**(2):357–372.
11. Baudin M, Berthon C, Coquel F, Masson R, Tran QH. A relaxation method for two-phase flow models with hydrodynamic closure law. *Numerische Mathematik* 2005; **99**(3):411–440.
12. Baudin M, Coquel F, Tran QH. A semi-implicit relaxation scheme for modeling two-phase flow in a pipeline. *SIAM Journal on Scientific Computing* 2005; **27**(3):914–936.
13. Evje S, Fjelde KK. Hybrid flux-splitting schemes for a two-phase flow model. *Journal of Computational Physics* 2002; **175**(2):674–701.
14. Evje S, Fjelde KK. On a rough AUSM scheme for a one-dimensional two-phase model. *Computers and Fluids* 2003; **32**(10):1497–1530.
15. Faille I, Heintzé E. A rough finite volume scheme for modeling two-phase flow in a pipeline. *Computers and Fluids* 1999; **28**(2):213–241.
16. Flåtten T, Munkejord ST. The approximate Riemann solver of Roe applied to a drift-flux two-phase flow model. Preprint available from http://www.rf.no/Internet/petroleum.nsf/p/205, 2005, submitted.
17. Chen GQ, Toro EF. Centered difference schemes for nonlinear hyperbolic equations. *Journal of Hyperbolic Differential Equations* 2004; **1**(3):531–566.
18. Toro EF, Billett SJ. Centred TVD schemes for hyperbolic conservation laws. *IMA Journal of Numerical Analysis* 2000; **20**(1):47–79.
19. Titarev VA, Toro EF. MUSTA schemes for multi-dimensional hyperbolic systems: analysis and improvements. *International Journal for Numerical Methods in Fluids* 2005; **49**(2):117–147.
20. Toro EF. Multi-stage predictor-corrector fluxes for hyperbolic equations. *Isaac Newton Institute for Mathematical Sciences Preprint Series*, University of Cambridge, U.K., NI03037-NPA, available from http://www.newton.cam.ac.uk/preprints2003.html
21. Zuber N, Findlay JA. Average volumetric concentration in two-phase flow systems. *Journal of Heat Transfer—Transactions of the ASME* 1965; **87**:453–468.
22. Hibiki T, Ishii M. Distribution parameter and drift velocity of drift-flux model in bubbly flow. *International Journal of Heat and Mass Transfer* 2002; **45**(4):707–721.
23. Titarev VA, Toro EF. Finite-volume WENO schemes for three-dimensional conservation laws. *Journal of Computational Physics* 2004; **201**(1):238–260.
24. Osher S. Convergence of generalized MUSCL schemes. *SIAM Journal on Numerical Analysis* 1985; **22**(5):947–961.
25. van Leer B. Towards the ultimate conservative difference scheme V. A second-order sequel to Godunov's method. *Journal of Computational Physics* 1979; **32**(1):101–136.
26. van Leer B. Towards the ultimate conservative difference scheme IV. New approach to numerical convection. *Journal of Computational Physics* 1977; **23**(3):276–299.
27. van Leer B. Towards the ultimate conservative difference scheme II. Monotonicity and conservation combined in a second-order scheme. *Journal of Computational Physics* 1974; **14**(4):361–370.
28. Ketcheson DI, Robinson AC. On the practical importance of the SSP property for Runge–Kutta time integrators for some common Godunov-type schemes. *International Journal for Numerical Methods in Fluids* 2005; **48**(3):271–303.
29. Liou MS. A sequel to AUSM: AUSM+. *Journal of Computational Physics* 1996; **129**(2):364–382.
30. Evje S, Flåtten T. Hybrid flux-splitting schemes for a common two-fluid model. *Journal of Computational Physics* 2003; **192**(1):175–210.
31. Harten A. High resolution schemes for hyperbolic conservation laws. *Journal of Computational Physics* 1983; **49**(3):357–393.

